Interaction of hydantoin with minority ions of solar wind: O^{6+} and He^{2+}

Julie Renoud,[a] Suvasthika Indrajith,[b] Alicja Domaracka,[b] Patrick Rousseau,[b] Patrick Moretto-Capelle,[a] Bernd A. Huber[b] and Jean-Philippe Champeaux[a]

The laboratory study of prebiotic molecules interacting with solar wind ions is essential to under- stand their role in the emergence of life in the complex context of astrochemistry of circumstellar environments. In this work, we present the first study of the interaction of hydantoin ($C_3N_2O_2H_4$, 100 amu) with Solar wind low energy multiply charged ions: O^{6+} at 30 keV and He^{2+} at 8 keV. The fragmentation mass spectra as well as correlation maps resulting from the collision are presented and discussed in this paper. Prompt and delayed dissosiation from metastable states of the ion- ized molelcule have been observed and corresponding life times mesured. Experimental results are completed by DFT numerical calculations of the energy and structures of the initial state of the molecule (z = 0,1,2,3) that show that the molecule can only support 2 charges before spon- taneously dissociate. Calculations also demonstrate that the hydantoin's ring opens after double ionisation of the molecule wich may enhance its reactivity in the context of biological molecule formation in crimcum stellar environnement. For the major experimentally observed fragmenta- tion pathways (like 44 amu / 56 amu dissociation), Internal Reaction Coordinate calculation was perfomed pointing out the important role of proton transfert in the fragmentation processes.

1 Introduction

Since the development of space telescopes and the rise of spatial infrared spectroscopy[1,2,3,4], numerous studies have noted the presence of neutral or cationic complex carbonaceous molecules in interstellar and circumstellar media, recorded in data bases such as[5,6,7]. Some are well identified by their spectral signatures like for example C_{60}^{+} or C_{70}^{+}[8,9,10] detected in the young planetary nebula TC1 and reflexion nebulae NGC7023, others are strongly suspected to be present in many nebulae as the family of Polycyclic Aromatic Hydrocarbons[11,12,13] but also organic species such as ethylene oxide[14]. The presence and richness of such molecular complexes reveal the possible existence of a physicochemistry in astrophysical environments related to their interactions with the ionizing radiation of the surrounding stars, either UV photons or stellar winds for circumstellar environments[15]. Organic and pre-biotic molecules have also been detected in several meteorites[16,17,18]. The presence of prebiotic molecules in the circumstellar environment raises the question of their interaction with solar wind particles and the role of theses interactions in the emergence of life.

In this context, we have focused on the 2,4-imidazolidinedione named hydantoin ($C_3N_2O_2H_4$, 100 amu). This prebiotic molecule has been detected in the Murchison and Yamato[19] meteorites and was synthesized in the laboratory in interstellar ice analogues irradiated by UV photons[20]. Even if hydantoin have not been yet detected directly in nebulae clouds or cometa ionic tails, the simplest amino acid glycine was clearly identified in 2016 in the comet 67P/Churyomov-Gerasimenko[21] ejecta and calculations showed[22] that hydantoin is a possible precursor of the amino acid glycine after hydrolysis. In the present work, we have looked at the collision induced dissociation of isolated neutral hydantoin by solar wind minority ions O^{6+} and He^{2+} at 30 keV and 8 keV kinetic energy respectively which correspond to an average solar wind speed of around 600 km.s^{-1}[23]. Obtained mass spectra are compared and discussed. Experimental results are completed by quantum chemistry calculations, for the singly and doubly charged hydantoin cation, in order to investigate fragmentation pathway for the most abundant fragments.

2 Experimental methods

The experiments were performed at the low-energy ion beam facility ARIBE of GANIL in Caen (France) with a crossed-beam device. The experimental setup is described in details elsewhere[24], thus, only a brief description is given here. Low–energy ions are produced in an electron cyclotron resonance ion source. They are

[a] *Laboratoire Collisions Agrégats et Réactivité, UMR 5589-CNRS Université Paul Sabatier Toulouse III, 118 Route de Narbonne, Bat 3R1B4, 31062 Toulouse Cedex 9, France.*

[b] *Normandie Univ, ENSICAEN, UNICAEN, CEA, CNRS, CIMAP, 14000 Caen, France.*

extracted, mass selected, pulsed (pulse length 1 μs) and transported to the experimental area, where they cross a molecular effusive beam evaporated from an oven device. After collimation, the different beam intensities are 250 pA for 8 keV $^3He^{2+}$ and 200-400 pA for 30 keV $^{16}O^{6+}$. After the interaction, cationic products are orthogonally extracted into a modified Wiley-McLaren linear time-of-flight TOF mass spectrometer[25]. After passing the 1m long drift region the mass-over-charge analyzed cations are strongly post-accelerated before impacting a conversion plate. Emitted secondary electrons are guided by a weak magnetic field towards a channel plate detector. In this way, high detection efficiency is obtained independently of the ion mass. The arrival times are digitized with 1 ns resolution in an event-by-event mode (FAST ComTec P7888). An event corresponds to one ion collision. Using a low intensity ion beam allows to obtain conditions where the number of charged particles produced within one ion pulse is negligibly small, thus several fragments detected per ion pulse are due to a single collision by event. Thus, each event is characterized by the number of detected fragments and their TOF values in such a way that the correlation between them can be studied[26]. The molecular beam was produced by evaporation of a commercial powder of hydantoin 98% purity purchased at Sigma-Aldrich in a heated oven. The oven temperature was kept at 393K to ensure sufficient vapor density and avoid thermal decomposition.

3 Quantum chemistry calculations of initials molecular structures

3.1 Initial molecular neutral structures

The neutral form of hydantoin $C_3N_2O_2H_4$ molecule in its fundamental state is presented in Figure 1:

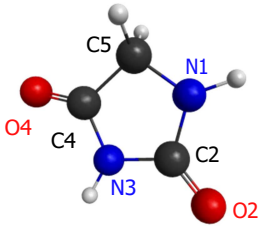

Fig. 1 Neutral form of Hyndatoin in the ground state (labels from[27]).

Geometry was optimized with the GAMESS code using the density functional theory (DFT), with the B3LYP functional and the 6-311G or 6-31G(d,p) basis set.

In our experimental setup, the temperature in the oven used to produce gas phase molecules is 393 K. If we suppose thermal equilibrium, this temperature corresponds to an internal energy given by:

$$E_{th} = (3N - 6)k_B T \quad (1)$$

With $N = 11$ (number of atoms) and $k_B = 8.617\,10^{-5}$eV.K^{-1}, this internal energy is then equal to 0.914 eV.

For such thermal energy we may expect that hydantoin molecule can form several tautomers during the heating of the powder in the oven. The ground state presents a keto group ($C^{(4)}O^{(4)}$ $C^{(2)}H_2$) and two lactam groups ($C^{(2)}O^{(2)}$ $N^{(3)}H$ and $C^{(2)}O^{(2)}$ $N^{(1)}H$). Proton transfer from N to O atoms and from CH_2 to CO may gives the lactims and enol tautomer, respectively.

In order to support this hypothesis, we have performed DFT calculations of these protomers with the same level of theory as used for the ground state . For each tautomer, we have evaluated the corresponding adiabatic energy ΔE as well as the activation barrier energy AE, referred to the neutral form (Figure 1). Results are presented in Figure 2, energies are given relatively to the ground state.

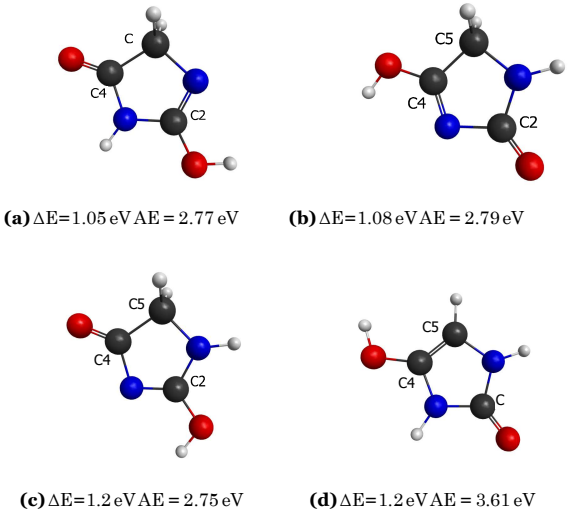

(a) ΔE=1.05 eV AE = 2.77 eV **(b)** ΔE=1.08 eV AE = 2.79 eV

(c) ΔE=1.2 eV AE = 2.75 eV **(d)** ΔE=1.2 eV AE = 3.61 eV

Fig. 2 Calculated geometries and energies of the tautomer form of the neutral hydantoin molecule. AE = activation barrier, ΔE = adiabatic energy.

Activation energy (AE) barriers corresponding to the transition state of theses tautomers are all more than 2 eV above the neutral form (see Figure 2). Thus, we can reasonably assume that proton transfers cannot be produced by the heating of the molecule during its sublimation but may only occur consecutively to the interaction with O^{6+} and He^{2+} ions.

3.2 Molecular excitation: Reachable charge states, energies and geometries

Vertical and adiabatic ionization energies relative to the ground state of the neutral molecule were calculated with the same functional as for the initial geometries calculation but using two basis sets: 6-311G and 6-31G(d,p). Results are given in Table 1.

Table 1 Calculated (B3LYP) ionisation energies of hydantoin

z	Vertical (eV)		Adiabatic (eV)	
	6-311G	6-31G(d,p)	6-311G	6-31G(d,p)
1	9.94	9.67	9.79	9.52
2	27.22	26.63	22.99	22.64
3	48.57	49.46	48.08	
3		50.79 (MP2)		44.14 (MP2)

For the 6-311G base, calculations are consistent with previous Bacchus-Montabonel[28] results at 9.91 eV and 9.60 eV for

the vertical and adiabatic ionisation respectively. The 6-31G(d,p) base gives lower energies than 6-311G basis set except for the hydantoin^{3+}. The difference between bases increases in absolute scale with the charge state from δE=0.27eV to 0.89 eV for vertical transitions. Calculation of the adiabatically relaxed Hyd^{3+} molecule does not converge using the DFT method. A stable geometry has been found using MP2 level of theory at 44.14 eV above neutral hydantoin.

The relaxed geometries of hydantoin obtained after Franck-Condon ionization from the ground state of the neutral molecule for the three reachable charge states are presented in Figure 3.

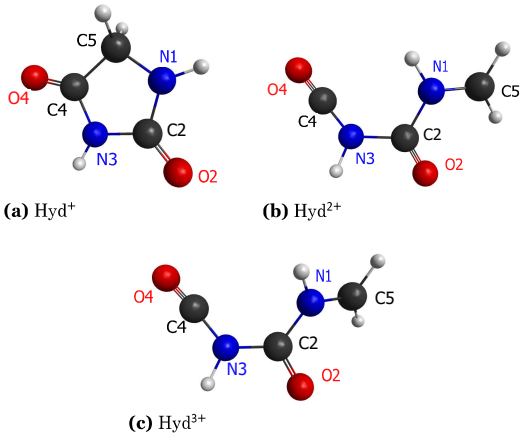

Fig. 3 Hyndatoin relaxed geometries for the different charge states of the molecule.

The hydantoin ring remains closed for z=1 but not for higher charge states. Calculations show that to reach the stable geometry of the hydantoin^{2+} from the vertical geometry the ring must open by breaking the $C^{(4)}$-$C^{(5)}$ bond. Calculations also show that the $C^{(2)}$-$N^{(1)}$ bond can easily rotate forming quasi energetically degenerated rotamers. This strong structural modification leads to a large energy difference between vertical and adiabatic states (4 eV in case of the dication and 6.7 eV in case of the trication (see Table 1). In this case, one may ask if the adiabatic states can be reached without any strong alteration. Dynamical Reaction Coordinates (DRC) calculations were then performed, initialised from the vertical geometry of the Hyd^{2+} and Hyd^{3+} ionized molecule.

Results are presented in Figure 4. For the dication (a) the ring open and the opened structure oscillates without breaking (calculation have been performed up to 10ps and no breaking occurs). Inversely, the trication (b) breaks into two charged fragments, namely 71^{2+} and 29^{+}. Therefore, theoretically, it should be possible to detect unfragmented Hyd^{2+} (m/z=50) but not Hyd^{3+} (m/z=33.3).

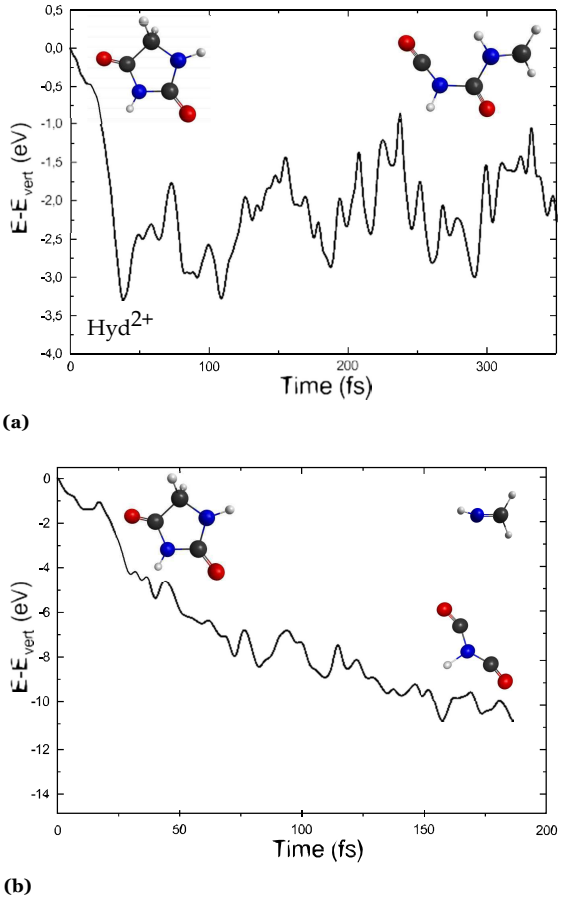

Fig. 4 DRC calculations (B3LYP, 6-31G(d,p)) from the vertical geometry of Hyd^{2+} (a) and Hyd^{3+} (b).

4 Experimental results and discussion

4.1 Dissociation mass spectra of hydantoin by stellar wind minority ions

If emitted in the gas phase in a circumstellar environment, the hydantoin molecule will interact with solar wind ions. From this interaction it can be multiply ionized due to electron capture and electronically excited if electron capture occurs from inner molecular orbitals. Non radiative relaxation like fragmentation and tauto-merisation can then occur:

$$\underset{100\,\mathrm{amu}}{C_3N_2O_2H_4} + X^{n+} \longrightarrow X^{(n-k)+} + (C_3N_2O_2H_4^{k+})^* \qquad (2)$$

$$\overrightarrow{\quad} \{A_i^{z_i+}\} + \{B_j^{0}\} \qquad (3)$$

With $\sum_i z_i = k$. The $\{A_i^{q_i+}\}$ cations produced in the interaction are mass/charge analysed by time of flight mass spectroscopy (see section 2). The corresponding spectra are presented in Figure 5, for both He^{2+} at 8 keV and O^{6+} at 30 keV.

The peak structure at m/z=100 corresponds to unfragmented parent hydantoin molecule labelled Hyd^{1+} in Figure 5. In both spectra, we observe a very weak signal of unfragmented Hyd^{2+} (m/z=50), with branching ratio 0.04% and 0.03% for He^{2+} and O^{6+}, respectively (see inset in Figure 5, corresponding to a zoom on the m/z=50 peak structure in the O^{6+} mass spectra). The ratio is quite low but it shows the existence of the stable hydantoin dictation at microsecond time scale corresponding to the time of flight duration. We do not observe in the mass spectrum Hyd^{3+} which would correspond to a peak structure at m/z=33.3. This indicates that the molecule dissociates easily when multiply charged. This is consistent with DRC calculations (see section 3),

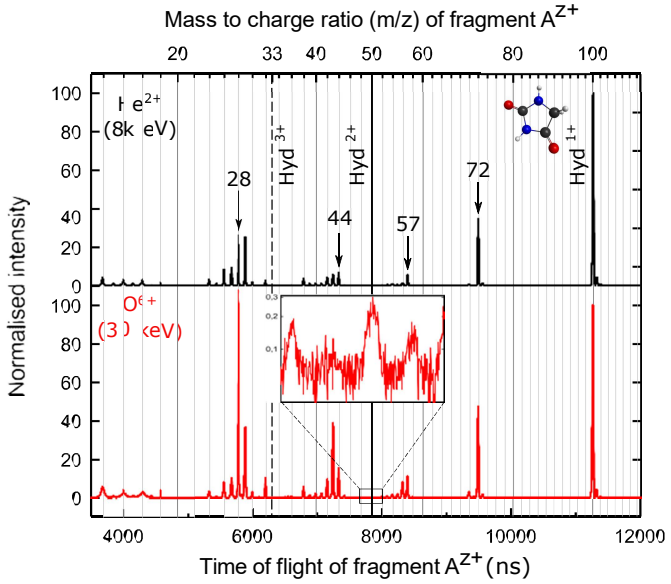

Fig. 5 Inclusive mass spectra of cations arising from the fragmentation of neutral hydantoin molecule $C_3N_2O_2H_4$ after collision with He^{2+} at 8 keV and O^{6+} at 30 keV. The inset is a zoom on the m/z=50 peak structure, corresponding to the unfragmented Hyd^{2+} parent ion (intensity is in log scale).

where we observe the possibility of non dissociation for Hyd^{2+} (with a strong structural change) and fragmentation for Hyd^{3+}.

The branching ratios are defined by:

$$\mu_i = \frac{\int_{t_1}^{t_2} S_{A_i}(\tau)d\tau}{\int_0^{t_f} S_{tot}(\tau)d\tau} \qquad (4)$$

where $S_{A_i}(\tau)$ and $S_{tot}(\tau)$ are the number of events in the time interval $d\tau$, for the peak structure corresponding to $A_i^{z_i+}$ fragment (between times t_1 and t_2) and for the total spectrum (between the spectrum time limits). They are given in Table 2 for the principal peak structures as well as relative intensity of each fragment compare to that of the unfragmented Hyd^{1+} and possible fragment identifications.

The branching ratio of unfragmented hydantoin molecule surviving the collision is lower in the case of O^{6+} (21.3%) than He^{2+} (40.2%), indicating that hydantoin molecules statistically dissociate more after 30 keV O^{6+} than 8 keV He^{2+} collisions. This can be attributed to higher instability due to higher molecular charge state produced in the collision with O^{6+}.

In terms of formed cations, both mass spectra for He^{2+} and O^{6+} are very similar with main fragmentation channels leading to m/z= 28, 29 and 72 cations (see Table 2).

4.2 Analysis of the main dissociation paths leading to mono cations

4.2.1 Fragment m/z=72

The formation of cations at m/z=72 implies the loss of a neutral mass 28 which can correspond to the fragment $C^{(2)}O^{(2)}$ or $C^{(4)}O^{(4)}$ (1 and 2 in Figure 5, with no molecular rearrangement) or the fragment CNH_2 including a proton transfer (from $C^{(5)}$ to $O^{(4)}$ or $N^{(1)}$ to $O^{(2)}$, indicated by 3b and 3a in Figure 6 respectively).

Table 2 Relative intensities and identification of the cationic products formed by collision of neutral hydantoin with He^{2+} at 8 keV and O^{6+} at 30 keV

m/z	He^{2+}		O^{6+}		Possible Id.
	μ_i (%)	Rel.	μ_i (%)	Rel.	
12	2,4	6.2	3,6	17.4	C^+
13	0,6	1.8	0,4	1.0	C^+
14	2,3	6.0	3,0	13.8	N^+/CH_2^+
15	0,6	1.8	0,6	0.9	N^+/NH^+
16	2,5	6.5	3,1	15.4	O^+
24	1,1	2.8	0,9	4.3	C_2^+
25	0,3	1.0	0,2	1.0	C_2H^+
26	2,7	6.9	2,0	9.8	$CN^+/C_2H_2^+$
27	3,1	7.9	2,4	11.4	CNH^+
27.5	0.04	0.1	x	x	C_2NOH^{2+}
28	8,2	20.5	20,5	93.9	CNH_2^+/CO
28.5	0.05	0.1	0.3	1.4	$C_2NOH_3^{2+}$
29	7,1	18.1	7,1	33.7	CNH_3^+/COH^+
30	0,6	1.7	0,6	3.1	CH_2O^+/NCH_4^+
35.5	0.02	0.05	0.14	0.6	$C_2N_2OH_4^{2+}/C_2NO_2H_2^{2+}$
38	1,3	3.3	1,0	5.2	C_2N^+
39	0,4	1.0	0,3	1.4	C_2NH^+
40	0,4	1.0	0,4	2.0	$C_2NH_2^+$
41	0,4	1.1	0,4	2.3	$C_2NH_3^+/C_2OH^+$
42	1,8	4.7	1,9	9.3	C_2OH_2/CNO^+
43	2,7	7.1	8,1	39.4	$CNOH^+$
44	2,2	5.6	3,0	14.2	$CNOH_2^+$
50	0.04	0.1	0.03	0.1	Hyd^{2+}
52	0,1	0.4	0,1	0.7	$C_2N_2^+$
53	0,2	0.6	0,2	1.1	$C_2N_2H^+$
54	0,4	1.2	0,4	2.2	$C_2NH_2^+/C_2NO^+$
55	0,1	0.5	0,4	2.4	C_2NOH^+
56	0,7	1.9	2,0	10.0	$C_2NOH_2^+$
57	1,8	4.6	2,1	10.2	$C_2NOH_3^+$
70	0,3	1.0	0,8	3.7	$C_2N_2OH_2^+$
72	12,3	30.6	9,3	43.4	$C_2N_2OH_4^+/C_2NO_2H_2^+$

$$C_3N_2O_2H_4^+ \longrightarrow C_2N_2OH_4^+ + CO \qquad (5)$$
(100 amu → 72 amu + 28 amu)

$$\longrightarrow C_2NO_2H_2^+ + CNH_2 \qquad (6)$$
(72 amu + 28 amu)

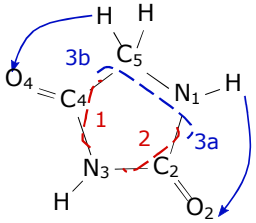

Fig. 6 Formation of m/z = 72 fragment via the loss of neutral CO (1 and 2) or neutral CNH_2 (3a and 3b).

A prompt emission is dominant but for both He^{2+} and O^{6+} spectra, we observe above peak at m/z=72 a decreasing tail to-

ward higher time of flight as shown in Figure 7.

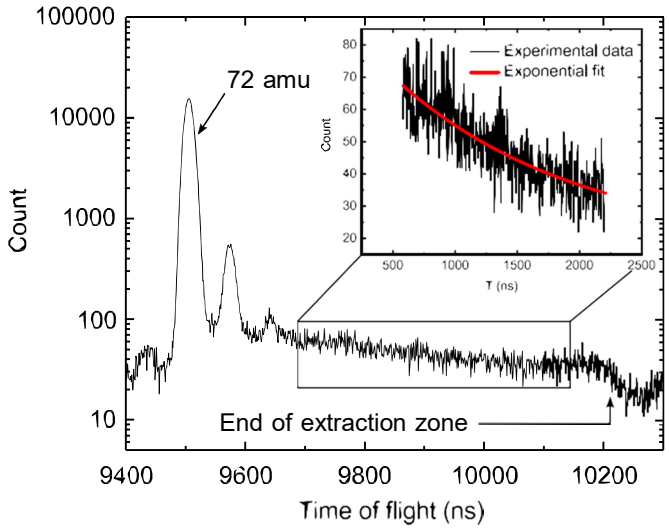

Fig. 7 Intensity distribution on the mass range around m/z =72 for He^{2+} projectile. The inset correspond to the delayed tail, fitted by an exponential. In this zoom, the time on abscissa axis is the delayed fragmentation time of the hydantoin molecule.

This tail is due to the delayed fragmentation of the hydantoin cation in the extraction zone of the mass spectrometer. The end of the decay tail correspond to the end of the extraction zone of the mass spectrometer (electric field = 24.4 $kV.m^{-1}$, length = 11 cm). Knowing the above decay process and the geometric and electronic configuration of the mass spectrometer, we can associate to each time of flight in the tail the corresponding time of residence of the unfragmented hydantoin cation in the mass spectrometer, that is to say its decay time. Zoom in Figure 7 shows the intensity in the tail as a function of the calculated decay time in the case of He^{2+} projectile. We observe an exponential decay $e^{-T/\tau}$ which leads to a lifetime for the hydantoin cation in the case of He^{2+} :

$$\tau_{He^{2+}} = (1.49 \pm 0.06)\ \mu s \qquad (7)$$

And in the case of O^{6+} :

$$\tau_{O^{6+}} = (2.30 \pm 0.13)\ \mu s \qquad (8)$$

A similar delayed fragmentation was observed in several mulecules after interaction with multiply charged low energy ions[29 30 31 32].

In order to investigate the origin of this meta-stability, we numerically looked at a possible reaction scheme for the emission of neutral mass 28 through a transition state. Calculations were performed in order to look for imaginary vibrational frequencies.

We found that the emission of neutral CNH_2 when formed after proton transfert occurs easily but does not go through a transition state which, considering Transition State Theory, forbids long meta-stability possibilities. Then, the CNH_2 fragment, if emitted, can only contribute to the prompt 72 amu peak signal.

After multiple numerical tentatives of neutral $C^{(2)}O^{(2)}$ emission via the opening of the $C^{(2)}$-$N^{(1)}$ or $C^{(2)}$-$N^{(3)}$ bonds, the Hyd^{1+} molecular ring always returns to the adiabatic geometry without dissociation. Only the emission of neutral $C^{(4)}O^{(4)}$ via the opening of the $C^{(4)}$-$N^{(3)}$ bond of hydantion ring followed by $C^{(5)}$-$C^{(4)}$ dissociation give rise to a transition state with an activation barrier compatible with the observed meta-stability. For this transition state, we performed an intrinsic reaction coordinate (IRC) calculation with the same level of theory as mentioned before (DFT B3LYP 6-31G(d,p)) to verify the connexion between minima. The corresponding fragmentation path is presented in Figure 8. The transition state is found at 1.86 eV above the adiabatic relaxed geometry of the Hyd^{1+} molecule. The dissociated state is only 0.32 eV lower than the transition state.

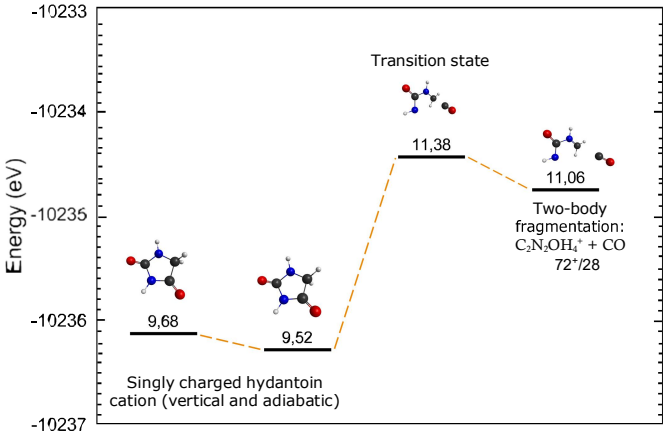

Fig. 8 Calculated two body fragmentation path leading to the formation of 72 amu cation via the loss of neutral $C^{(4)}O^{(4)}$. Energies levels are referenced against the neutral hydantoin molecule.

The observed differences between the Hyd^{1+} life time in the case of O^{6+} at 30keV and He^{2+} at 8 keV can result from differences in the internal energy deposited by both projectiles in the molecule. Indeed, considering Transition State Theory [33], the lifetime τ (inverse of the unimolecular reaction rate k) can be express as a function of temperature T following:

$$k = \frac{1}{\tau} = \frac{1}{h} k_B T \frac{Q_{TS}(T)}{Q_{init}(T)} e^{-\frac{\Delta E}{k_B T}} \qquad (9)$$

where $Q_{TS}(T)$ and $Q_{init}(T)$ are the partition functions of the transition state and initial state respectively. ΔE is the activation barrier (energy between the optimized hydantoin singly charged cation and the transition state). For a molecule with N atoms, total partition functions are given by: $Q_{TOT} = Q_{vib}Q_{rot}$ with vibrational and rotational partition functions respectively, defined as:

$$Q_{vib} = \prod \frac{1}{1 - e^{-\frac{h\nu_i}{k_B T}}} \qquad (10)$$

$$Q_{rot} = \frac{\left(\frac{2k_B T}{\hbar^2}\right)^{1/2} \left(\pi I_x I_y I_z\right)^{1/2}}{\sigma} \qquad (11)$$

Vibrational frequencies ν_i for each mode and moments of inertia in each direction I_x, I_y and I_z are given by GAMESS numerical calculation, for both initial and transition state. Finding the temperature which solves eq. 9 for each lifetime gives the internal energy $U = (3N - 6)k_B T$ of the molecule: 2.36 eV for O^{6+} and

2.42eV for He^{2+}. Even if this difference between internal energies are small compared to the difference between the lifetimes (due to the exponential parts of eq. 9), this is consistent with a simple Classical Over-the-Barrier model (COB)[34]. This model supposes that electron transfer from a molecule to the projectile can occur when the maximum of potential barrier created by the two point charges is lower or equal to the Stark shifted ionisation potential of the molecule. This condition leads to a minimal radius R_n to capture the n^{th} electron given by:

$$R_n = \frac{2(q+n-1)^{1/2}n^{1/2}+n}{I_n^*} \qquad (12)$$

Where n is the ionisation state of the molecule, q is the initial charge of the projectile (6 for O and 2 for He) and $I_n^* = I_n + (q-n+1)/r$ is the n^{th} Stark shifted ionisation potential of the molecule (I_n is the n^{th} non-shifted ionisation potential and r is the distance between target and projectile). Calculated R_n for hydantoin molecule and the two projectiles are given in Table 3.

Table 3 Radii of n^{th} electron capture from hydantoin to He^{2+} and O^{6+}, classical over the barrier calculation

	He^{2+}	O^{6+}
n	R_n (a_0)	R_n (a_0)
1	10.6	16.3
2	4.8	8.3
3	∅	5.5
4	∅	3.6
5	∅	2.6
6	∅	1.8

Thus, the COB model predicts that O^{6+} will be able to capture more electrons from the target molecule and as the radius of capture is larger than for He^{2+}, less energy will be transfered to the molecule.

4.2.2 Cationic fragments m/z=28 and m/z=29

The fragment with m/z=28 is one of the predominant fragments for both He^{2+} and O^{6+}, leading to neutral undetected fragments. A natural way to produce m/q = 28 would be the loss of $C^{(4)}O^{(4)}$ (Fragment 1 in Figure 9a) or $C^{(2)}O^{(2)}$ (Fragment 2 in Figure 9a). Taking into account the possible proton transfer from $C^{(5)}$ to $O^{(4)}$ or $N^{(1)}$ to $O^{(2)}$ (Figure 2a and 2c repectively), the peak at 28 amu may also correspond to CHNH (Fragment 3b in Figure 9a) or CH_2N (Fragment 3a in Figure 9a) cation, respectively.

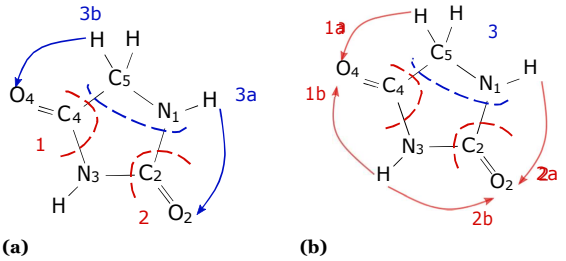

Fig. 9 Location of fragment m/q = 28 (a) and fragment m/q = 29 (b) comming from Hyd^{1+} cation.

Energy calculations of the dissociation energies, have shown that in case of CO, a fragmentation in $72^+ + 28$ is energetically lower (1.9 eV and 2.1 eV above Hyd^{1+} cation for $C^{(4)}O^{(4)}$ and $C^{(2)}O^{(2)}$ respectively) than a fragmentation in $72 + 28^+$ (6.9 eV and 8.1 eV above Hyd^{1+} cation for $C^{(4)}O^{(4)}$ and $C^{(2)}O^{(2)}$ respectively). In case of both CHNH and CH_2N, the fragmentation leading to $72 + 28^+$ is energetically lower (5.2 eV and 6.7 eV above Hyd^{1+} tautomer cation for CHNH and CH_2N respectively) and occurs without transition state (exept the proton transfer in case of CHNH). Fragmentation in $72^+ + 28$ was found to be 12.9 eV and 10.7 eV above Hyd^{1+} tautomer cation for CHNH and CH_2N respectively. These results, displayed in Table 4, indicate that fragments with m/z = 28 coming from fragmentation of the hydantoin monocation are more likely $CHNH^+$ or CH_2N^+ than CO^+. Another way to form m/z = 28 fragment is a multistep fragmentation, as a CO or CHNH group is often found at the end of higher mass fragments (e.g.: 57 amu: $N^{(1)}H$-$C^{(5)}H2$-$C^{(4)}O^{(4)}$ or $C^{(5)}H2$-$N^{(1)}H$-$C^{(2)}O^{(2)}$, 44 amu: $N^{(3)}H$-$C^{(4)}O^{(4)}$ or $N^{(3)}H$-$C^{(2)}O^{(2)}$). As discussed later, the 28 amu fragment may also be formed via direct or multistep fragmentation of multiply charged ions ($N^{(1)}H$-$C^{(5)}H2$ (29 amu) and $C^{(4)}O^{(4)}$ (28 amu) are localized at the extremities of the doubly ionized hydantoin (see Figure 3b)).

Table 4 Dissociation limits for fragmentations $Hyd^+ \rightarrow 72^{(+)} + 28^{(+)}$. Energies are in eV and referenced against Hyd^+ stable or corresponding proton transfer tautomer

	$72^+ + 28$	$72 + 28^+$
$C^{(4)}O^{(4)}$	1.9	6.9
$C^{(2)}O^{(2)}$	2.1	8.1
CH–NH	12.9	5.2
CH_2-N	10.7	6.7

The fragment with m/z=29 is identified as $C^{(2)}O^{(2)}H$ (proton transfer from $N^{(1)}$ to $O^{(2)}$ or $N^{(3)}$ to $O^{(2)}$, see 2a and 2b respectively in Figure 9b), $C^{(4)}O^{(4)}H$ (proton transfer from $N^{(3)}$ to $O^{(4)}$ or $C^{(5)}$ to $O^{(4)}$ see 1a and 1b respectively in Figure 9b) or CH_2–NH with no proton transfer (see 3 in Figure 9b). Calculated dissociation limits relative to the Hyd^+ cation (stable or totaumer), are presented in Table 5. The only case where a fragmentation $71 + 29^+$ is energetically advantageous corresponds to the loss of $C^{(2)}O^{(2)}H$. However, energy differences are significantly lower than for the 28 amu fragment. This indicates that part of the peak structure at m/z =29 coming from Hyd^+ fragmentation is preferentially due to the $C^{(2)}O^{(2)}H$ ion but may also contain $C^{(4)}O^{(4)}H$ and CH_2NH^+ ions. As for the 28 amu fragment, the 29 amu may also be produced by delayed fragmentation or dication fragmentation.

4.3 Analysis of the main dissociation path leading to dication and correlated singly charged cations

Interaction of neutral hydantoin with Solar wind ions may also lead to dicationic Hyd^{2+} ion (see section 3) and dicationic fragments A^{2+}. Fragmentation of these dications may contribute to the monocation intensity.

Inclusive mass spectra (i.e fragments from the Hyd^{k+} molecule whatever the initial charge k is) reveals for both ions some small peaks at m/z=27.5, 28.5 and 35.5(branching ratio 0.04, 0.05,

Table 5 Dissociation limits for fragmentations $Hyd^+ \rightarrow 71^{(+)} + 29^{(+)}$. Energies are in eV and referenced against Hyd^+ stable or corresponding proton transfer tautomer

Proton transfert	$71^+ + 29$		$71 + 29^+$
		CH_2NH	
	3.6		4.6
		$C^{(4)}O^{(4)}H$	
$N^{(3)} \rightarrow O^{(4)}$	3.7		4.3
$C^{(5)} \rightarrow O^{(4)}$	5.7		8.5
		$C^{(2)}O^{(2)}H$	
$N^{(1)} \rightarrow O^{(2)}$	5.8		5.6
$N^{(3)} \rightarrow O^{(2)}$	5.9		5.8

0.02 and 0, 0.29, 0.14 for He^{2+} and O^{6+} respectively). These non-integer m/z peaks can be unambiguously related to $A^{2+} = 55^{2+}, 57^{2+}, 71^{2+}$ ions. Zoom on Figure 5 corresponding to these m/z is shown in Figure 10.

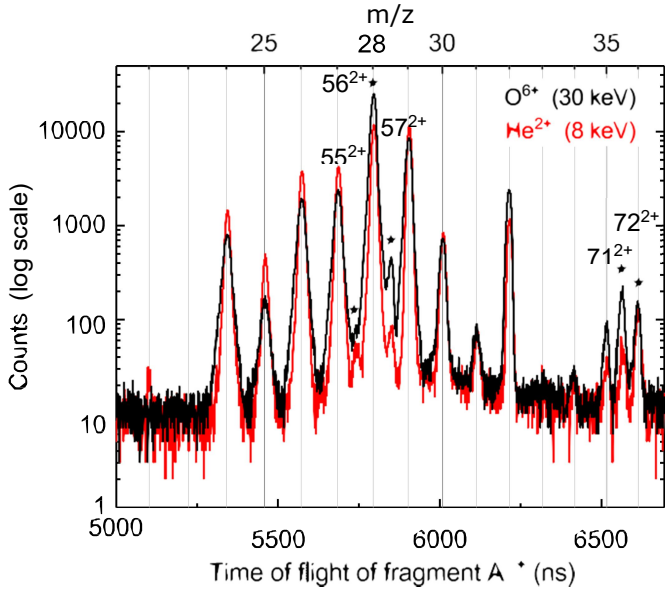

Fig. 10 Zoom on the inclusive spectra arising from the fragmentation of charged hydantoin molecule after collision with He^{2+} at 8 keV and O^{6+} at 30 keV. Peaks corresponding to doubly charged fragments are labelled by stars.

In case of fragmentation with charge separation, coincidence measurements of A^+/B^+ charged fragments have been performed for each collision event. The Table 6 summarizes the branching ratio (normalized to the whole intensity of the correlated spectrum) of the most intense A^+/B^+ coincidences experimentally observed after double ionisation of hydantoin molecule.

Table 6 Branching ratio of the major correlation of two mono cations after double ionisation of neutral hydantoin molecule by He^{2+} at 8 keV and O^{6+} at 30 keV

A^+/B^+	He^{2+} (%)	O^{6+} (%)
$44^+/56^+$	5	7
$28^+/43^+$	8	20
$(27^+ \rightarrow 29^+)/(42^+ \rightarrow 44^+)$	20	38

Corresponding correlation maps are presented in Figure 11 (a) for He^{2+} projectile and 11(b) for O^{6+}.

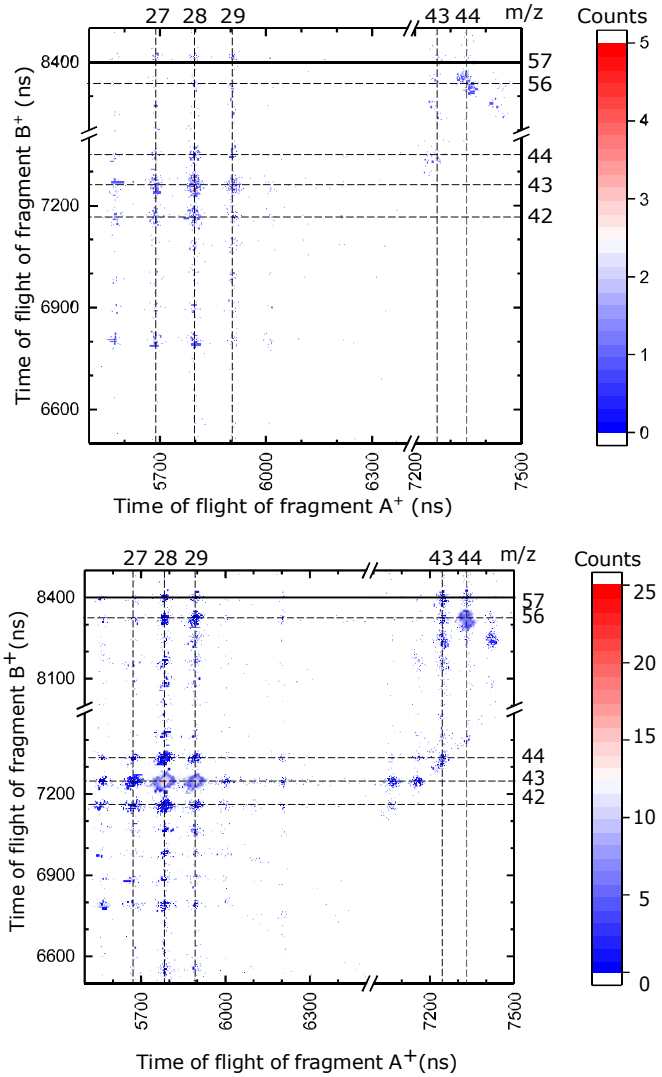

Fig. 11 Map of the correlation between A^+ and B^+ fragments, corresponding to the fragmentation of the hydantoin dication after collision with He^{2+} at 8 keV (a) and O^{6+} at 30 keV (b).

The most intense correlation corresponds to $A^+/B^+ = (43 \pm 1)^+ / (28 \pm 1)^+$ fragments for both solar wind ions with an important branching ratio difference between O^{6+} and He^{2+} for $28^+/43^+$ correlation at 20% and 8%, respectively.

4.3.1 Dication $A^{2+} = 71^{2+}$

The 71^{2+} (m/q=35.5 amu) fragment can be attributed to $O^{(4)}C^{(4)}N^{(3)}HC^{(2)}O^{(2)\,2+}$, via the loss of neutral $N^{(2)}HC^{(5)}H_2$ (29 amu) from the initial Hyd^{2+} ion as shown in Figure 12a.

DFT (B3Lyp 6-31G(d,p)) geometry optimization of the 71^{2+} dication shows that a stable symmetric structure exists (see Figure 12b). No correlation involving $71^{2+}/B^+$ were observed but intense correlation $28^+/43^+$ could be linked to the observed 71^{2+} dication.

4.3.2 $28^+/43^+$ correlation

Calculation reveals the existence of a transition state with activation barrier of 4.7eV that can lead to the dissociation of the

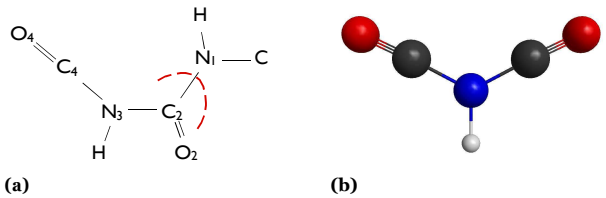

Fig. 12 (a) Localisation of the 71 amu fragment on the hydantoin molecule dication (b) Optimized geometry (numerical calculation) of the 71^{2+} fragment.

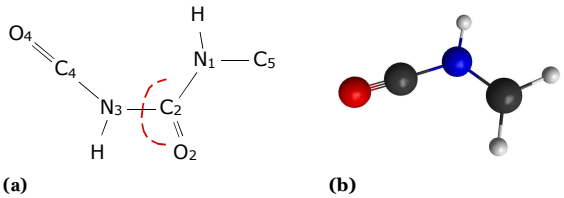

Fig. 14 (a) Localisation of the 57 amu fragment on the hydantoin molecule dication (b) Optimized geometry (numerical calculation) of the 57^{2+} fragment.

primarily formed 71^{2+} into CO^+(28 amu) and $HNCO^+$(43 amu). The corresponding calculated reaction pathway is presented in Figure 13.

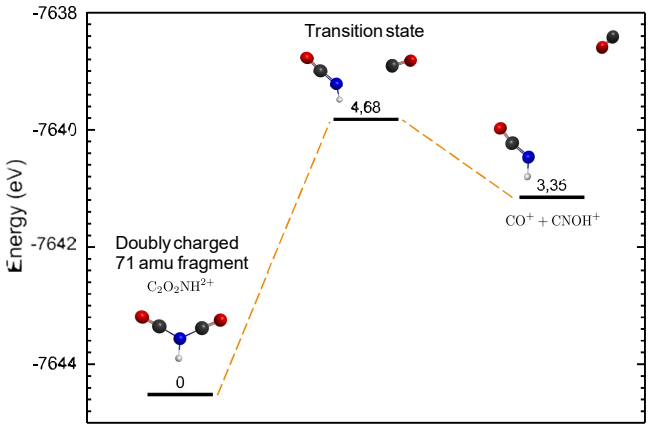

Fig. 13 Calculated fragmentation path from 71^{2+} to $28^+ + 43^+$. Energies levels are in eV and referenced against 71^{2+} optimized geometry.

Figure 10 shows that the branching ratio of 71^{2+} is higher in case of O^{6+} than He^{2+}. The lack of 71^{2+} in case of He^{2+} may suggest that it dissociate more easily in $28^+ + 43^+$. In this case, an increasing of peak 28 amu should be observed in the He^{2+} spectrum, which is not the case (see Figure 10), but this contribution is certainly overlapped by the fragmentation after single capture.

Another way to form $28^+/43^+$ correlation would be via initial charge separation:

$$\underset{100\ \text{amu}}{C_3N_2O_2H_4^{2+}} \longrightarrow \underset{57\ \text{amu}}{C_2NOH_3^{+}} + \underset{43\ \text{amu}}{CNOH^+} \qquad (13)$$

$$\longrightarrow \underset{29\ \text{amu}}{CNH_3} + \underset{28\ \text{amu}}{CO^+} + \underset{43\ \text{amu}}{CNOH^+} \qquad (14)$$

A low correlation signal is observed for $43^+/57^+$ masses, corresponding to this charge separation (see Figure 11).

4.3.3 Dications $A^{2+} = 55^{2+}$ and $A^{2+} = 57^{2+}$

The 57^{2+} fragment, arising from Hyd^{2+} fragmentation, can correspond to C_2NOH_3 (without rearrangement, see Figure 14a) and a stable structure for the dication have been found (see Figure 14b).

The fragment 55^{2+} corresponds to the loss of two hydrogen atoms (from CH_2 group) from the 57^{2+} fragment. The smaller intensity of 55^{2+} compared to 57^{2+} can be related to the higher order process. The loss of one hydrogen should be more probable and conducts to the formation of 56^{2+}, unfortunately, it cannot be sociate in $28^+ + (28 \pm 1)^+$, leading to $28^+/(28 \pm 1)^+$ correlations, and participating to 28 amu peak structure. Indeed, a weak signal is observed in the O^{6+} correlation map, but not enough data were recorded for He^{2+} to observe this correlation island.

4.3.4 Two body fragmentation: $44^+/56^+$ correlation

One of the most intense A^+/B^+ correlation with both projectile corresponds to a two body fragmentation of Hyd^{2+}(50 amu) forming two mono-cations 44^+ amu and 56^+ amu (upper right corner of Figure 11 a) and b)).

Surprisingly, this rather intense process implies a proton transfer in the Hyd^{2+} molecule before the two body fragmentation is able to form the masses 44 and 56 amu. We then examined a reaction scheme that could lead to this dissociation using the DFT calculation for geometric optimizations and internal reaction coordinate calculations in order to connect the different geometries of each state involved in the dynamics of the dissociation. Results of these calculations are presented Figure 15.

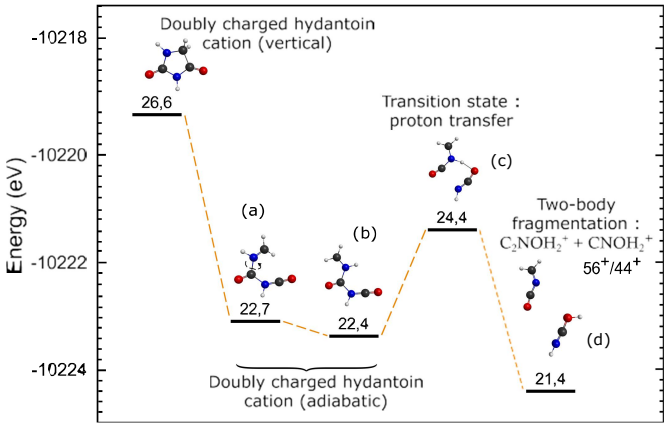

Fig. 15 Calculated fragmentation path corresponding to the two body Hyd^{2+} to $44^+ + 56^+$. Energies levels are in eV and referenced against neutral hydantoin optimized geometry.

As discussed in 3.2, the vertical dication geometry relaxes by opening the $C^{(4)}C^{(5)}$ bond, to form the (a) geometry in Figure 16. A rotamer is then formed via a low transition state (not indicated in Figure 16), by rotating $N^{(1)}H\text{-}C^{(5)}H_{(2)}$ group. This stable rota-

tional isomer (b) is 0.2 eV below stable dication. From this Hyd^{2+} geometry, a 2 eV transition state (c) leads to a proton transfer from $N^{(1)}$ to $O^{(4)}$ and immediate dissociation in $56^+ + 44^+$, see Figure 16.

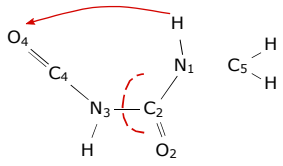

Fig. 16 Two body fragmentation $Hyd^{2+}(100^{2+}) \rightarrow 56^+ + 44^+$, via a proton transfer.

5 Conclusion

In this work, we report on the fragmentation of the prebiotic molecule hydantoin ($C_3N_2O_2H_4$, 100 amu) after collisions with multiply charged minority ions of Solar wind: He^{2+} at 8kev and O^{6+} at 30keV. Experimental results, obtained at Ganil, are supported by numerical calculations. For both projectiles, major fragments were found at 28, 43 and 72 amu, identified as CNH_2^+, $CNOH^+$ and $C_2N_2OH_4^+$, respectively. The role of proton transfer was clearly established in the case of two body dication fragmentation $44^+/56^+$. Due to the very low amount of unfragmented Hyd^{2+} parent dication and the absence of unfragmented Hyd^{3+}, we conclude, in consistence with numerical calculations, that the hydantoin molecule does not resist to charge. This fragility makes the transportation of hydantoin from a circumstellar environment to Earth in gas form in comet outgassing difficult. The fact that the hydantoin geometry is opening when doubly charged implies a high reactivity of the hydantoin dication and makes it interesting for physico-chemistry of circumstellar media, even if no fragments involved in the synthetising of the amino acid glycine have been found in mass spectra. In the following, we would like to study the fragmentation of the hydantoin molecule induced by interacting with majority components of Solar wind: protons and electrons.

Conflicts of interest

There are no conflicts to declare.

Acknowledgements

We would like to thank the EMIE research group (GDR 4479) for participating financially in the measurements campaign carried out on Cimap's facilities in Caen, France. We also thank the selection committee of Cimap for accepting our proposal and all Cimap staff for their welcome and support in carrying out these experiments.

Notes and references

1 T. de Graauw, L. N. Haser, D. A. Beintema, P. R. Roelfsema, H. van Agthoven, L. Barl, O. H. Bauer, H. E. G. Bekenkamp, A.-J. Boonstra, D. R. Boxhoorn, J. Cote, P. de Groene, C. van Dijkhuizen, S. Drapatz, J. Evers, H. Feuchtgruber, M. Frericks, R. Genzel, G. Haerendel, A. M. Heras, K. A. van der Hucht, T. van der Hulst, R. Huygen, H. Jacobs, G. Jakob, T. Kamperman, R. O. Katterloher, D. J. M. Kester, D. Kunze, D. Kussendrager, F. Lahuis, H. J. G. L. M. Lamers, K. Leech, S. van der Lei, R. van der Linden, W. Luinge, D. Lutz, F. Melzner, P. W. Morris, D. van Nguyen, G. Ploeger, S. Price, A. Salama, S. G. Schaeidt, N. Sijm, C. Smoorenburg, J. Spakman, H. Spoon, M. Steinmayer, J. Stoecker, E. A. Valentijn, B. Vandenbussche, H. Visser, C. Waelkens, L. B. F. M. Waters, J. Wensink, P. R. Wesselius, E. Wiezorrek, E. Wieprecht, J. J. Wijnbergen, K. J. Wildeman and E. Young, *Astronomy and Astrophysics*, 1996, L49–L54.

2 J. R. Houck, T. L. Roellig, J. v. Cleve, W. J. Forrest, T. Herter, C. R. Lawrence, K. Matthews, H. J. Reitsema, B. T. Soifer, D. M. Watson, D. Weedman, M. Huisjen, J. Troeltzsch, D. J. Barry, J. Bernard-Salas, C. E. Blacken, B. R. Brandl, V. Charmandaris, D. Devost, G. E. Gull, P. Hall, C. P. Henderson, S. J. U. Higdon, B. E. Pirger, J. Schoenwald, G. C. Sloan, K. I. Uchida, P. N. Appleton, L. Armus, M. J. Burgdorf, S. B. Fajardo-Acosta, C. J. Grillmair, J. G. Ingalls, P. W. Morris and H. I. Teplitz, *The Astrophysical Journal Supplement Series*, 2004, **154**, 18.

3 M. W. Werner, T. L. Roellig, F. J. Low, G. H. Rieke, M. Rieke, W. F. Hoffmann, E. Young, J. R. Houck, B. Brandl, G. G. Fazio, J. L. Hora, R. D. Gehrz, G. Helou, B. T. Soifer, J. Stauffer, J. Keene, P. Eisenhardt, D. Gallagher, T. N. Gautier, W. Irace, C. R. Lawrence, L. Simmons, J. E. V. Cleve, M. Jura, E. L. Wright and D. P. Cruikshank, *The Astrophysical Journal Supplement Series*, 2004, **154**, 1.

4 G. L. Pilbratt, J. R. Riedinger, T. Passvogel, G. Crone, D. Doyle, U. Gageur, A. M. Heras, C. Jewell, L. Metcalfe, S. Ott and M. Schmidt, *Astronomy & Astrophysics*, 2010, **518**, L1.

5 *Interstellar Molecules - The Cosmic Ice Laboratory - Sciences and Exploration Directorate - NASA's Goddard Space Flight Center*, `https://science.gsfc.nasa.gov/691/cosmicice/interstellar.html`.

6 *Cometary Molecules - The Cosmic Ice Laboratory - Sciences and Exploration Directorate - NASA's Goddard Space Flight Center*, `https://science.gsfc.nasa.gov/691/cosmicice/cometary.html`.

7 *Molecules in Space | I. Physikalisches Institut*, `http://www.astro.uni-koeln.de/cdms/molecules`.

8 J. Cami, J. Bernard-Salas, E. Peeters and S. E. Malek, *Science*, 2010, **329**, 1180–1182.

9 E. K. Campbell, M. Holz, D. Gerlich and J. P. Maier, *Nature*, 2015, **523**, 322–323.

10 K. Sellgren, M. W. Werner, J. G. Ingalls, J. D. T. Smith, T. M. Carleton and C. Joblin, *EAS Publications Series*, 2011, **46**, 209–214.

11 A. Leger and J. L. Puget, *Astronomy and Astrophysics*, 1984.

12 C. Boersma, A. L. Mattioda, C. W. Bauschlicher, E. Peeters, A. G. G. M. Tielens and L. J. Allamandola, *The Astrophysical Journal*, 2008, **690**, 1208–1221.

13 E. Peeters, C. Bauschlicher, L. J. Allamandola, A. G. G. M. Tielens, A. Ricca and M. G. Wolfire, *The Astrophysical Journal*, 2017, **836**, year.

14 J. E. Dickens, W. M. Irvine, M. Ohishi, M. Ikeda, S. Ishikawa,

A. Nummelin and . Hjalmarson, *The Astrophysical Journal*, 1997, **489**, 753.

15 J.-P. Champeaux, P. Moretto-Capelle, P. Cafarelli, C. Deville, M. Sence and R. Casta, *Monthly Notices of the Royal Astronomical Society*, 2014, **441**, 1479–1487.

16 G. W. Cooper and J. R. Cronin, *Geochimica et Cosmochimica Acta*, 1995, **59**, 1003–1015.

17 P. Ehrenfreund and S. B. Charnley, *Annual Review of Astronomy and Astrophysics*, 2000, **38**, 427–483.

18 A. S. Burton, J. C. Stern, J. E. Elsila, D. P. Glavin and J. P. Dworkin, *Chemical Society Reviews*, 2012, **41**, 5459–5472.

19 A. Shimoyama and R. Ogasawara, *Origins of life and evolution of the biosphere*, 2002, **32**, 165–179.

20 P. De Marcellus, M. Bertrand, M. Nuevo, F. Westall and L. D'hendecourt, *Astrobiology*, 2011, **11**, 847–54.

21 K. Altwegg, H. Balsiger, A. Bar-Nun, J.-J. Berthelier, A. Bieler, P. Bochsler, C. Briois, U. Calmonte, M. R. Combi, H. Cottin, J. D. Keyser, F. Dhooghe, B. Fiethe, S. A. Fuselier, S. Gasc, T. I. Gombosi, K. C. Hansen, M. Haessig, A. Jäckel, E. Kopp, A. Korth, L. L. Roy, U. Mall, B. Marty, O. Mousis, T. Owen, H. Rème, M. Rubin, T. Sémon, C.-Y. Tzou, J. H. Waite and P. Wurz, *Science Advances*, 2016, **2**, e1600285.

22 M. Kayanuma, K. Kidachi, M. Shoji, Y. Komatsu, A. Sato, Y. Shigeta, Y. Aikawa and M. Umemura, *Chemical Physics Letters*, 2017, **687**, 178–183.

23 R. von Steiger, N. A. Schwadron, L. A. Fisk, J. Geiss, G. Gloeckler, S. Hefti, B. Wilken, R. R. Wimmer-Schweingruber and T. H. Zurbuchen, *Journal of Geophysical Research: Space Physics*, 2000, **105**, 27217–27238.

24 T. Bergen, X. Biquard, A. Brenac, F. Chandezon, B. A. Huber, D. Jalabert, H. Lebius, M. Maurel, E. Monnand, J. Opitz, A. Pesnelle, B. Pras, C. Ristori and J. C. Rocco, *Review of Scientific Instruments*, 1999, **70**, 3244–3253.

25 F. Chandezon, B. Huber and C. Ristori, *Review of Scientific Instruments*, 1994, **65**, 3344–3353.

26 M. Capron, S. Díaz-Tendero, S. Maclot, A. Domaracka, E. Lattouf, A. Ławicki, R. Maisonny, J.-Y. Chesnel, A. Méry, J.-C. Poully, J. Rangama, L. Adoui, F. Martín, M. Alcamí, P. Rousseau and B. A. Huber, *Chemistry – A European Journal*, 2012, **18**, 9321–9332.

27 F.-L. Yu, C. H. Schwalbe and D. J. Watkin, *Acta Crystallographica Section C: Crystal Structure Communications*, 2004, **60**, o714–o717.

28 M.-C. Bacchus-Montabonel, *Chemical Physics Letters*, 2016, **664**, 173–177.

29 K. Takahashi, K. Yokokawa, A. Mizumura, J. Matsumoto, H. Shiromaru, H. Kumar, P. Bhatt and C. P. Safvan, *Physical Review A*, 2018, **98**, 062708.

30 V. Bernigaud, *phdthesis*, Université de Caen, 2009.

31 J. Kocisek, D. G. Piekarski, R. Delaunay, B. A. Huber, L. Adoui, F. Martín, M. Alcamí, P. Rousseau, A. Domaracka, J. Kopyra and S. Díaz-Tendero, *The Journal of Physical Chemistry A*, 2015, **119**, 9581–9589.

32 S. Indrajith, P. Rousseau, B. A. Huber, C. Nicolafrancesco, A. Domaracka, K. Grygoryeva, P. Nag, B. Sedmidubská, J. Fedor and J. Kočišek, *The Journal of Physical Chemistry C*, 2019.

33 R. G. Gilbert and S. C. Smith, *Theory of unimolecular and recombination reactions.*, Oxford, Blackwell Scientific Publications, 1990.

34 A. Bárány, G. Astner, H. Cederquist, H. Danared, S. Huldt, P. Hvelplund, A. Johnson, H. Knudsen, L. Liljeby and K. G. Rensfelt, *Nuclear Instruments and Methods in Physics Research Section B: Beam Interactions with Materials and Atoms*, 1985, **9**, 397–399.